iScience

CellPress
OPEN ACCESS

Article

A functional role for glycosylated B7-H5/VISTA immune checkpoint protein in metastatic clear cell renal cell carcinoma

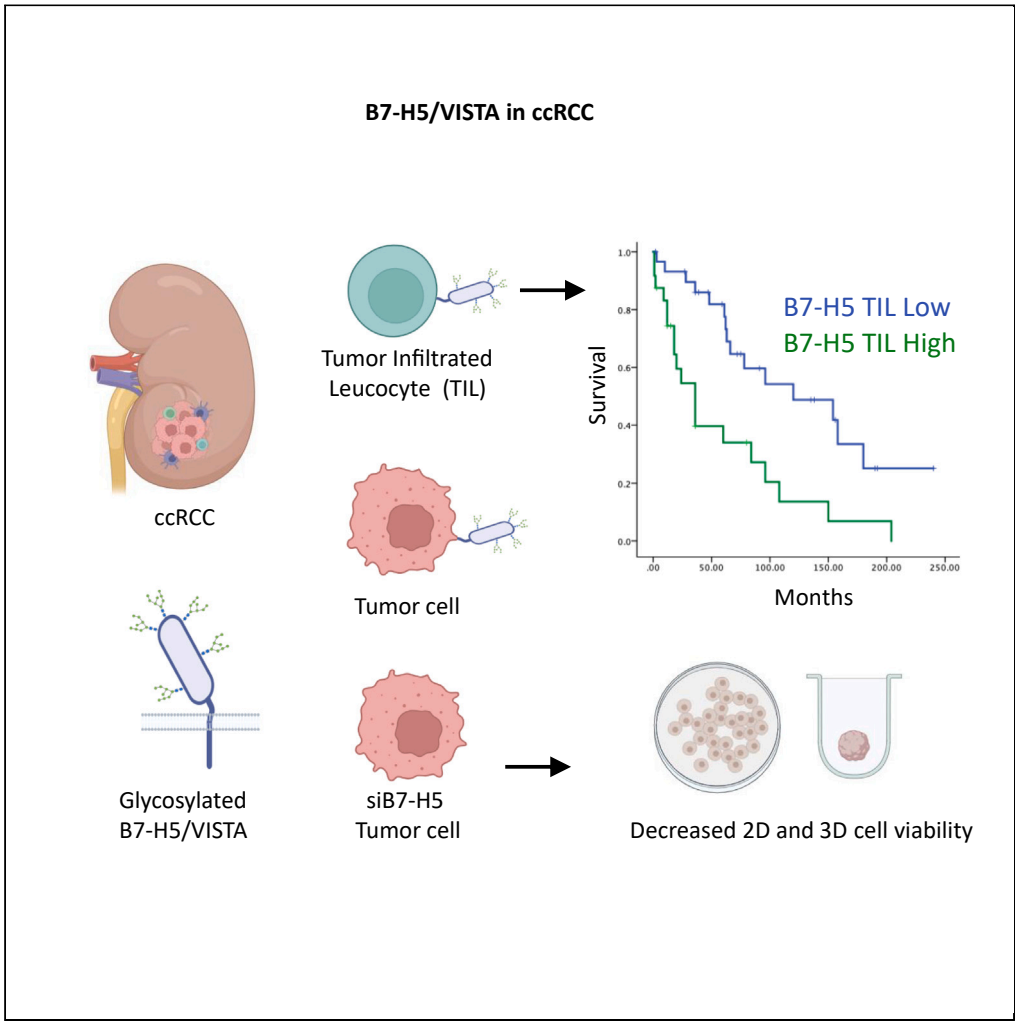

Maite Emaldi, Paula Alamillo-Maeso, Esther Rey-Iborra, ..., Rafael Pulido, José I. López, Caroline E. Nunes-Xavier

carolinenunesxavier@gmail.com

Highlights

Mutagenic studies on B7-H5 identified the residues targeted by glycosylation

B7-H5 N-glycosylation revealed an impact on protein expression levels and localization

Knockdown of B7-H5 expression decreased 2D and 3D viability of renal cancer cells

B7-H5 expression on TILs correlated with poor outcomes in ccRCC

Emaldi et al., iScience 27, 110587
September 20, 2024
https://doi.org/10.1016/j.isci.2024.110587

iScience

CellPress
OPEN ACCESS

Article

A functional role for glycosylated B7-H5/VISTA immune checkpoint protein in metastatic clear cell renal cell carcinoma

Maite Emaldi,[1,2] Paula Alamillo-Maeso,[1] Esther Rey-Iborra,[1,2] Lorena Mosteiro,[1,2,3] David Lecumberri,[1,4] Rafael Pulido,[1,2,5] José I. López,[1] and Caroline E. Nunes-Xavier[1,2,6,7,*]

SUMMARY

Increased expression of the B7 family of immune checkpoint proteins hinders tumor elimination by the immune system. Expression levels of the B7-H5 protein were found to be upregulated in clear cell renal cell carcinomas (ccRCC). We here report the molecular, functional, and clinical characterization of B7-H5 from renal cancer cells and metastatic ccRCC tumors. B7-H5 was highly glycosylated and mainly expressed in the cell membrane. Mutagenic studies on B7-H5 identified the residues targeted by N-glycosylation and revealed an impact of B7-H5 glycosylation on protein expression levels and localization. B7-H5 knockdown decreased the cell proliferation and viability of renal cancer cells. We analyzed B7-H5 expression on tumor cells and tumor-infiltrated leukocytes (TILs) in samples from metastatic ccRCC patients and found that B7-H5 expression on TILs correlated with syncronous metastases and poor outcomes. These results provide insights into the molecular properties and clinical impact of B7-H5 and support B7-H5 as a new immunotherapeutic target in metastatic ccRCC.

INTRODUCTION

Cancer progression occurs via different processes that include cell death resistance, metastasis, and evasion of immune-mediated destruction. During cancer development, there is a dynamic period named immunoediting, in which immune cells may eliminate tumor cells. However, cancer cells are able to evade immune elimination via different mechanisms. This paradigm can be divided into three phases: elimination, equilibrium, and evasion. Firstly, cells that have undergone mutations that are not repaired by DNA repair mechanisms are identified and eliminated by the immune system (cancer immuno-surveillance); secondly, tumor cells that have not been eliminated by lymphocytes display restrained growth by the immune system; and thirdly, the lack of control by the immune system enables cancer cells to avoid recognition and elimination leading to tumor growth and metastasis.[1,2] This capacity of the tumor cells to avoid immune attack is one of the main characteristics of cancer pathogenesis and can be carried out by different mechanisms, including the ability of cancer cells to express immune checkpoint proteins on the cell surface. Therefore, understanding the interaction between cancer development and the immune system is essential to improve current therapies and implement new ones.

The V-domain immunoglobulin suppressor of T cell activation (VISTA), or B7-H5 (official gene name, *VSIR;* GenBank: NM_022153), is an inhibitory B7 family member that under physiological conditions maintains T cell and myeloid quiescence. Under inflammatory conditions, however, B7-H5 induces myeloid cells to reduce the expression of pro-inflammatory cytokines by reducing Toll-like receptor (TLR) signaling and it also increases the release of anti-inflammatory mediators.[3–5] B7-H5 can bind to V-set and Ig domain-containing 3 (VSIG-3) and to P-selectin glycoprotein ligand 1 (PSGL-1) ligands, probably with bidirectional signaling. Therefore, it can act both as a ligand and a receptor. In both interactions, pH is an important regulatory factor, being the interaction with PSGL-1 favored by the acidic pH in the tumor microenvironment (TME).[6,7] Additional B7-H5 binding partners include VSIG-8 and the metalloproteinase MMP-13, among others (reviewed in[8,9]).

B7-H5 is a glycosylated type I transmembrane protein that shares structural features with B7 and CD28 protein families and shares sequence homology with both PD-1 and PD-L1. Different from other B7 family members, B7-H5 only contains one single large N-terminal IgV-like domain. The cytoplasmic domain has three C-terminal Src homology domain 3 (SH3) binding motifs and one Src homology domain 2 (SH2) binding motif, several casein kinase 2 and protein kinase C phosphorylation sites, and a potential ubiquitylation site.[10,11] As other

[1]Department of Cancer, Biobizkaia Health Research Institute, 48903 Barakaldo, Spain
[2]CIBERER, ISCIII, 28029 Madrid, Spain
[3]Department of Pathology, Cruces University Hospital, 48903 Barakaldo Bizkaia, Spain
[4]Service of Urology, Hospital de Urduliz, 48610 Urduliz, Spain
[5]Ikerbasque, Basque Foundation for Science, 48009 Bilbao, Spain
[6]Department of Tumor Biology, Institute for Cancer Research, Oslo University Hospital Radiumhospitalet, 0424 Oslo, Norway
[7]Lead contact
*Correspondence: carolinenunesxavier@gmail.com
https://doi.org/10.1016/j.isci.2024.110587

members from the B7-homologous family, B7-H5 does not contain immunoreceptor tyrosine-based signaling motifs (ITAM/ITIM motifs) in its cytoplasmic domain.[12]

B7-H5 is mostly expressed in hematopoietic tissues and on the myeloid and lymphoid compartments. In tumors, B7-H5 is expressed on myeloid-derived suppressive cells, tumor-infiltrating leukocytes (TILs), and antigen-presenting cells,[10,11,13] and it has been reported increased B7-H5 expression in tumor-infiltrated hematopoietic cells after anti-CTLA-4/anti-PD-1 treatment, possibly due to adaptive resistance to immune checkpoint blockade.[14,15] In addition, soluble forms of B7-H5 have been detected which are increased in the serum of patients with distinct cancers, and associated with high-stage and metastases.[16,17] Less commonly, B7-H5 can also be expressed on tumor cells varying across cancer types. High expression of B7-H5 has been associated with poor prognosis in several human cancers, including ccRCC, making B7-H5 a suitable target for immunotherapy.[18–21] In this regard, antibody blockade of B7-H5 by antagonist antibodies inhibits regulatory T cell immunosuppressive functions, and several of these antibodies are currently under preclinical development in cancer models, including combinatory therapies with antibodies against PD-1, CTLA-4, and PD-L1.[5,9,22,23] In addition, global glycoproteomic analysis of ccRCC unveiled the potential of protein glycosylation in ccRCC development,[24] however little is known about the glycosylation pattern of B7-H5 in renal cells.

The evolving therapeutic landscape of ccRCC includes immune checkpoint inhibitors in combination with targeted therapies, and despite its constant improvement, there is a need for alternative therapeutic modalities to improve efficacy, toxicities, response rates, and quality of life.[4,25,26] B7-H5 is upregulated at both mRNA and protein levels in ccRCC tumors compared to normal adjacent tissues. Furthermore, B7-H5 expression in ccRCC tumors correlated with poor T cell responses, and blockade of B7-H5 with anti-B7-H5 antibody in *in vivo* mouse experiments decreased RCC tumor growth.[20] In ccRCC with venous tumor thrombus, B7-H5 high expression in tumor-infiltrated leukocytes correlated with metastasis and with decreased overall survival.[27] Here, we present the molecular, functional, and clinical characterization of B7-H5 in renal cancer cells. A positive role for highly glycosylated B7-H5 in renal cancer cell proliferation is disclosed, and we report the correlation of B7-H5 high expression in TILs with poor prognosis in metastatic ccRCC. Our findings suggest a role for B7-H5 in metastatic ccRCC and support the notion of B7-H5 as a suitable new target for ccRCC immunotherapy.

RESULTS

Characterization and localization of glycosylated B7-H5

The comparison of the mRNA expression levels of B7-H5 in ccRCC tumor and normal renal tissues shows the upregulated expression of B7-H5 in ccRCC, suggesting a positive role for B7-H5 in ccRCC progression (Figure 1A). To characterize the B7-H5 protein, Western blot analysis was performed with total lysates from renal HEK293 cells transfected with pcDNA3.1+/C-DYK containing B7-H5 Flag (C-terminal Flag epitope tagging), and ectopic expression was visualized using anti-Flag antibody (Figure 1B). A cluster of protein bands was identified as B7-H5. We hypothesized that the larger-molecular weight range of bands (40–58 kDa) could correspond to different forms of glycosylated B7-H5 protein, whereas the smaller-molecular weight band (36.5 kDa) could correspond to the non-glycosylated form of the protein. Next, to study the subcellular localization of B7-H5, immunofluorescence assays were performed with HEK293 and COS-7 cells transfected to ectopically express B7-H5 Flag and localization of the proteins was visualized by confocal microscopy using an anti-Flag antibody (Figure 1C). In both HEK293 and COS-7 cells, the B7-H5 Flag protein was distributed mainly in the plasma membrane, with some cytoplasmic staining (Figure 1C).

To study the glycosylation of B7-H5, total lysates from HEK293 cells ectopically expressing B7-H5 Flag were treated with PNGase F endoglycosidase, which hydrolyses N-glycan chains from proteins. Western blot was performed and the migration of proteins was analyzed using anti-Flag and anti-B7-H5 antibodies (Figure 1D). Treatment with PNGase F shifted the migration of B7-H5 Flag proteins from the high molecular weight range (40–58 kDa) to the low molecular weight range (36.5 kDa) confirming that B7-H5 protein is heavily N-glycosylated. A similar migration pattern was observed for untagged B7-H5, as detected with anti-B7-H5 antibody (Figures 1E and 1F). Accordingly, further experiments were made ectopically expressing untagged B7-H5 in renal cells.

To identify potential N-glycosylated residues in B7-H5 protein sequence, we performed an *in silico* analysis using the online web server NetNGlyc, and six potential N-glycosylation motifs (Asn-Xxx-Ser/Thr; N-X-S/T) were found at residues N49, N91, N108, N128, N135, and N190 (Figures 2A and 2B). Next, site-directed mutagenesis was performed to create B7-H5 variants mutating to Ala (A) these Asn residues: N49A, N91A, N108A, N128A, N135A, and N190A, alone or in combinations. Western blot analysis was performed with total lysates from HEK293 cells ectopically expressing B7-H5 wild type (WT) or N/A variants. Protein bands corresponding to B7-H5 N49A, N91A, N108A, N128A, and N135A migrated at lower molecular weight than B7-H5 WT, indicating that N49, N91, N108, N128, and N135 are B7-H5 N-glycosylation sites. B7-H5 N190A migrated similarly to B7-H5 WT, suggesting that N190 is not targeted by N-glycosylation. Analysis of multiple N/A compound mutations revealed an additive effect on the migration of B7-H5 protein. In addition, B7-H5 protein expression levels were gradually diminished in the N/A compound mutations, in a manner dependent on multiple N-glycosylated residues (Figure 2C). This suggests that the lack of N-glycosylation affects the stability of B7-H5 proteins.

Next, immunofluorescence assays were performed in HEK293 cells ectopically expressing B7-H5 N/A mutations to study whether N-glycosylation affected its subcellular localization. All single B7-H5 N/A mutations, and 2-to-4 residues compound N/A mutations (N2-N4), were mainly distributed in the cell membrane with some cytoplasmic distribution, similar to B7-H5 WT. However, when all 5 N-glycosylated residues (N5) were mutated, the localization was not seen in the membrane and was mainly cytoplasmic (Figure 3).

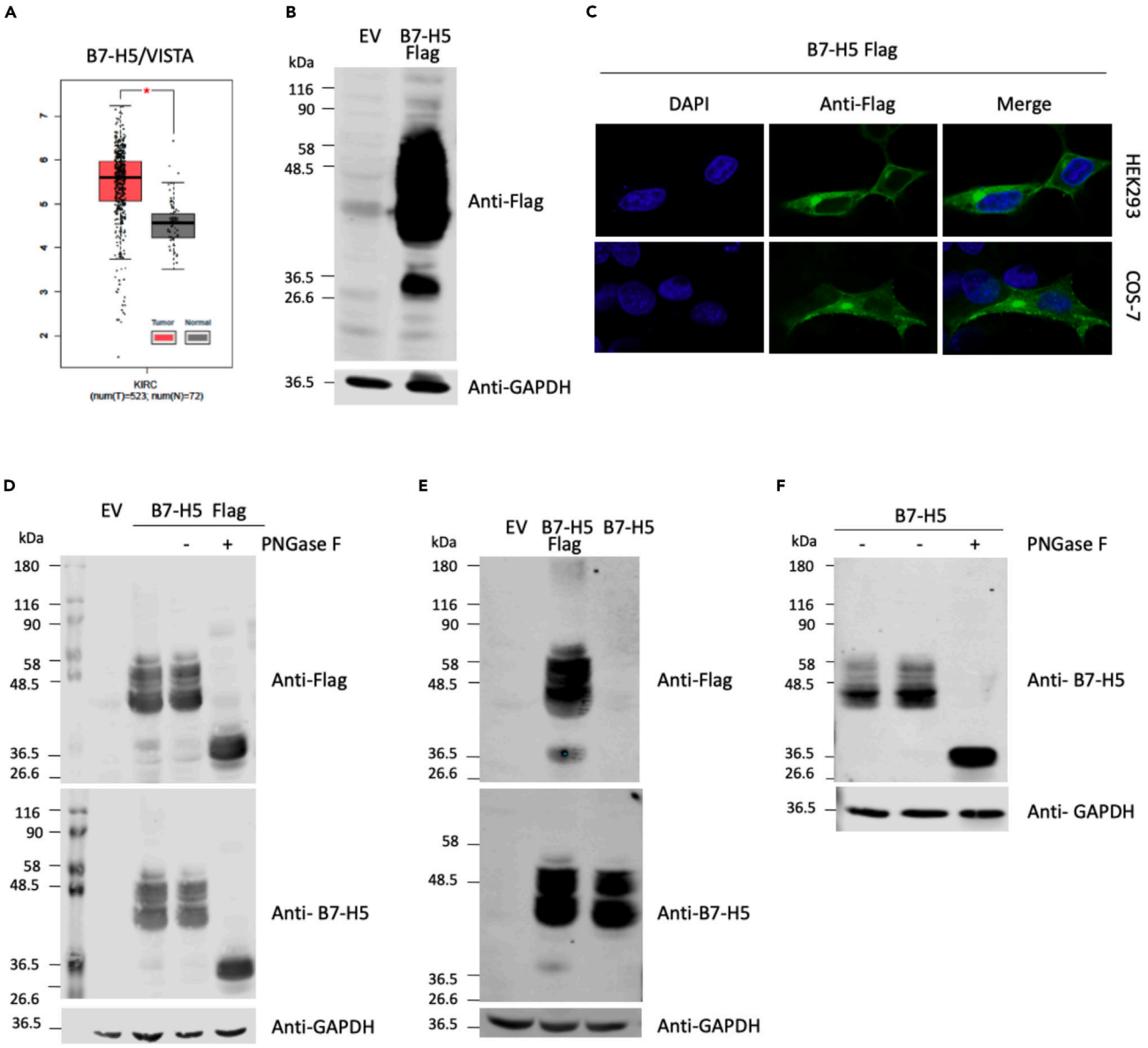

Figure 1. Expression and biochemical characterization of B7-H5 in renal cells

(A) Boxplot of B7-H5/VISTA mRNA expression in ccRCC tumor tissue (shown in red) in comparison to normal tissue (in gray). Data are represented in a logarithmic scale (Log2) and obtained from 523 tumor samples and 72 normal tissue samples (data from TCGA). The asterisk indicates a statistically significant difference ($p < 0.01$).

(B) Western blot of total lysates from HEK293 cells ectopically expressing B7-H5 Flag. Cells were transfected with pcDNA3.1+/C-DYK empty vector (EV) or containing B7-H5 Flag, and a Western blot was performed using anti-Flag or anti-GAPDH (loading control) antibodies. Migration of molecular weight markers is shown.

(C) Immunofluorescence confocal microscopy images at 63X showing subcellular localization of ectopically expressed B7-H5 Flag in HEK293 and COS-7 cells. Anti-Flag primary antibody and Alexa Fluor 488-conjugated secondary antibody were used for visualization of B7-H5 Flag (in green). Nuclei were stained with DAPI (in blue).

(D) Western blot of total lysates from HEK293 cells ectopically expressing B7-H5 Flag. Cells were transfected with pcDNA3.1+/C-DYK empty vector (EV) or containing B7-H5 Flag. Lysates were kept untreated or processed for PNGase F protocol in the absence (–) or in the presence of PNGase F enzyme (+). Western blot was performed using anti-Flag, anti-B7-H5, or anti-GAPDH antibodies. Migration of molecular weight markers is shown.

(E) Western blot of total lysates from HEK293 cells ectopically expressing B7-H5 Flag or B7-H5. Cells were transfected with pcDNA3.1+/C-DYK empty vector (EV), or containing B7-H5 Flag or B7-H5. Western blot was performed using anti-Flag, anti-B7-H5, or anti-GAPDH antibodies. Migration of molecular weight markers is shown.

(F) Western blot of total lysates from HEK293 cells ectopically expressing B7-H5.Lysates were kept untreated or treated with PNGase F, as indicated. Anti-B7-H5 was used for identification of B7-H5 protein and anti-GAPDH was used as a loading control.

Functional role of B7-H5 in renal cancer cells

The proliferation and viability of renal cancer cells were studied after silencing of B7-H5 expression with different siRNAs, using non-specific siRNA (siNS) as a negative control. Firstly, 786-O and Caki-1 renal cancer cells were transfected with four different B7-H5 siRNAs, RNA was isolated and retro transcribed, and real-time quantitative polymerase chain reaction (RT-qPCR) was performed to test the efficacy of the silencing (Figure S1). In both cell lines siB7-H5 #1 and siB7-H5 #4 showed more efficiency for the silencing of B7-H5, and were selected for further functional assays. Next, the proliferation and viability of 786-O and Caki-1 cells were monitored by proliferation and viability assays after silencing of B7-H5 expression with siB7-H5 #1 and siB7-H5 #4. Silencing of B7-H5 expression in both renal cancer cell lines resulted in a modest, but significant, decrease of 2D cell proliferation (Figure 4A). B7-H5 expression was also silenced in 786-O and Caki-1 cell spheroids using siB7-H5#1 and siB7-H5#4. The evolution of the 3D spheroids was observed and photographed daily. The spheroid area decreased after silencing with both siRNAs (Figure 4B). To further verify the functional effect of B7-H5 silencing in 3D models, cell viability was measured and compared to the negative control (siNS). In spheroids of both cell lines, silencing of B7-H5 significantly reduced 3D cell viability and showed a more prone effect than differences in proliferation measured by 2D (Figure 4C).

Clinical impact of B7-H5 expression in metastatic clear cell renal cancer carcinomas

To gain further insights into the clinical impact of B7-H5 protein expression in ccRCC, we evaluated by IHC the expression of B7-H5 in tumor samples from a retrospective cohort of 54 metastatic ccRCC patients (Table 1). Expression was scored as negative (when low or no staining) or positive (when moderate or high staining) (see details in STAR methods section). Representative immunostaining images are shown in Figure 5. We observed expression of B7-H5 protein on tumor cells in 13/54 (24%) cases and on TILs in 24/54 (44%). B7-H5 expression displayed a major cytoplasmic/membranous localization. We analyzed the clinicopathological correlations of B7-H5 expression on tumor cells and TILs. We found a significant negative correlation of high B7-H5 expression in the tumor cells with lower grades (Table 1). Significant correlations were also found of B7-H5 expression on TILs with the stage ($p = 0.033$), necrosis ($p = 0.004$), sarcomatoid transformation ($p = 0.020$), disease-free survival ($p = 0.015$), synchronous metastasis (p 0.000) (Table 1), and correlation to metastasis to non-epithelial organs ($p = 0.037$) (Table 2). Importantly, we found a significant positive correlation of B7-H5 TIL immunostaining with lower overall survival ($p = 0.027$).

Kaplan–Meier curves for survival time and expression of B7-H5 on TILs showed significant correlations with overall survival (log rank test, $p = 0.001$) (Figure 6, upper panels). In addition, Kaplan–Meier curves for time to first metastasis and expression of B7-H5 on TILs showed differential significant correlations (log rank test, $p = 0.005$) (Figure 6, lower panels). Cox regression multivariate analysis, including statistically significant variables and variables previously shown to be clinically relevant, revealed that the necrosis and B7-H5 on TILs were independent prognostic parameters for the overall survival of metastatic ccRCC patients in this cohort ($p = 0.019$ and $p = 0.002$, respectively) (Table 3). Sarcomatoid transformation, metastasis synchronicity, and B7-H5 expression on tumor cells were excluded from the predictive model because they did not significantly correlate with patient survival (Table 3).

DISCUSSION

Increased expression of B7 immune checkpoint proteins on tumors evade elimination by the immune system. Some members of the B7 family are highly expressed in different types of cancer and immune cells, playing a role in cancer progression and immune evasion, in correlation with poor prognosis. This outlines B7 family members as new potential biomarkers and therapeutic targets in cancer, although knowledge on these proteins is limited.[12] Currently, immune checkpoint inhibitors are in clinical use to target some of these proteins, which promotes T cell-mediated tumor elimination. Although ccRCC is a particularly chemo- and radio-resistant cancer, targeted therapies and PD-1/PD-L1-based immunotherapies have shown promising results.[22,29] Nevertheless, many patients do not respond or develop resistance over time, possibly due to the co-expression of other checkpoint proteins in the tumor microenvironment.[30] As a consequence, there is a need to identify better biomarkers as well as new therapeutic targets for ccRCC. The aim of this work was to characterize B7-H5 immune checkpoint proteins in ccRCC as a potential biomarker for high-risk ccRCC.

In silico analysis showed that B7-H5 mRNAs are upregulated in ccRCC bulk tumor tissue. In RCC, it has been reported that the activity of HIF is increased via the mTOR pathway and the inactivation of *VHL*,[31] and HIF induced hypoxia in the TME upregulates B7-H5 expression in colorectal cancer.[32] B7-H5 protein was recently found upregulated in tumor cells from patients with ccRCC, and its expression correlated with poor T cell responses.[33] High expression of B7-H5 in ccRCC progression could be linked to VHL and HIF signaling and requires further studies.

In our study, we did not detect endogenous B7-H5 expression in ccRCC, HEK293 or COS-7 cell lines, suggesting low levels of protein expression. Since ccRCC cell lines were not efficiently transfected with plasmid-based cDNA, B7-H5 biochemical characterization was performed on transiently transfected HEK293 cells. Our analysis led to the identification of two different clusters of B7-H5 protein bands that corresponded to N-glycosylated forms of B7-H5 (40–58 kDa) and non-glycosylated B7-H5 (36.5 kDa), as indicated by treatment with PNGase F endoglycosidase. Similar protein patterns have been described for PD-L1, where a cluster of bands at 50 kDa corresponds to the PD-L1 N-glycosylated form of the protein, and the PD-L1 non-glycosylated form is detected at 33 kDa.[34,35] IHC and immunofluorescence assays on cells overexpressing B7-H5 revealed that B7-H5 is distributed mainly at the cell membrane but also in the cytoplasm, consistent with previous reports.[36] Site-directed mutagenesis was performed to create B7-H5 variants targeting potential N-glycosylation sites (B7-H5 N49A, N91A, N108A, N128A, N135A, N190A). Our analysis indicates that N49, N91, N108, N128, and N135, but not N190, are B7-H5 N-glycosylation sites and that single mutations alone do not alter significantly B7-H5 protein expression nor subcellular localization. However, multiple mutations showed a gradual impact of N-glycosylation on both protein expression levels and protein localization. In this regard, it

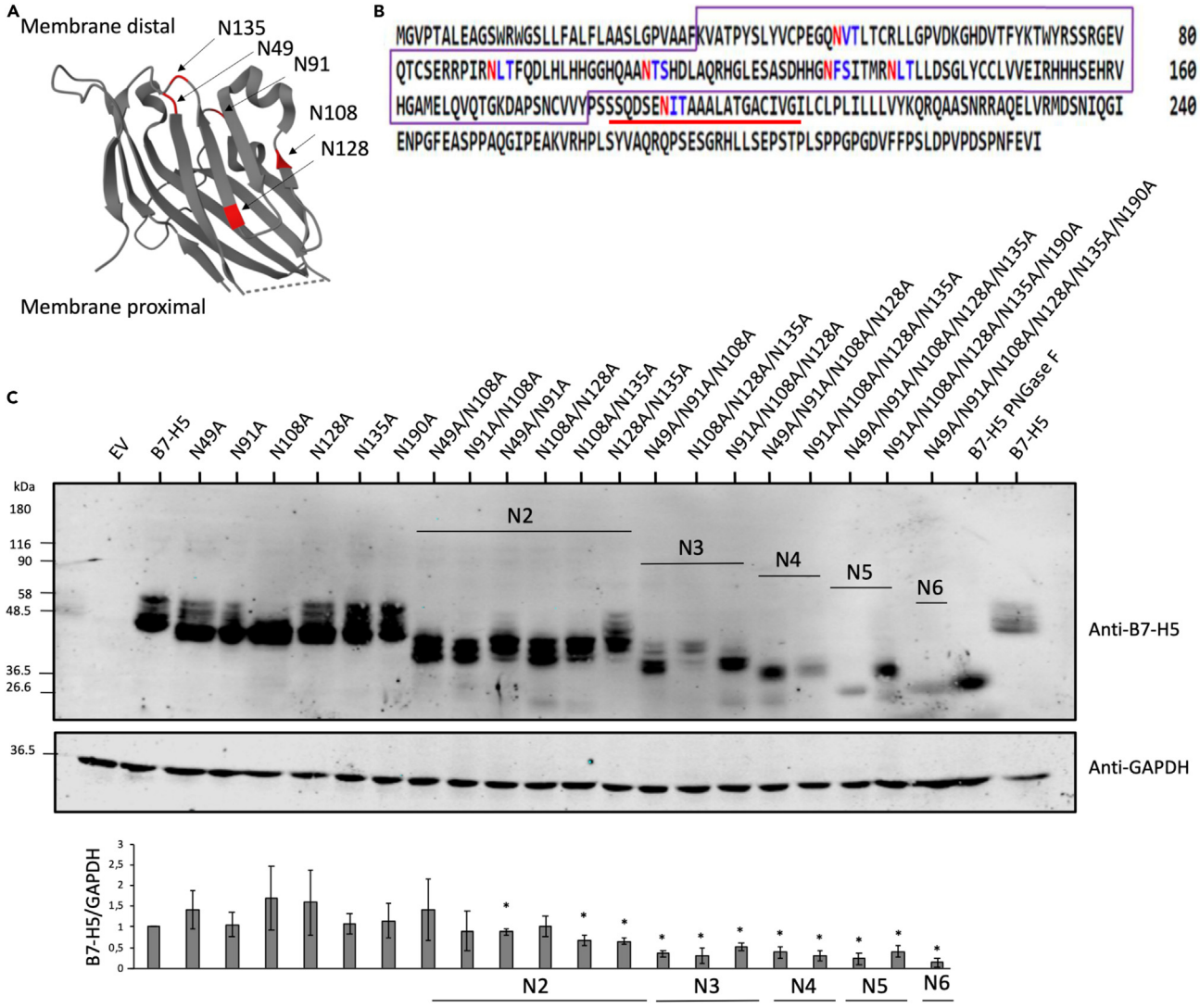

Figure 2. N-glycosylation sites of B7-H5

(A) Depiction of B7-H5 3D structure and localization of the amino acids targeted by glycosylation in the extracellular region (N49, N91, N108, N128, N135). Extracellular domain of B7-H5 is shown according to accession 6OIL.[28] Crystal structure visualization by Protein DataBank. N-glycosylated sites are highlighted in red.

(B) Potential N-glycosylation sites in B7-H5 protein sequences (NP_071436.1). Asn/N that have a high probability of being N-glycosylated are shown in red, whereas Asn/N that have a lower probability of being N-glycosylated are shown in blue. IgV domain is highlighted in a violet box, and transmembrane region is underlined in red.

(C) Western blot of total lysates from HEK293 cells ectopically expressing B7-H5, B7-H5 N49A, N91A, N108A, N128A, N135A, N190A single and multiple mutations (N2-N6), as indicated. Cells were transfected with pcDNA3.1+/C-DYK empty vector (EV), or with B7-H5 variants. B7-H5 WT lysate was kept untreated or treated with PNGase F, as indicated. Anti-B7-H5 was used for identification of B7-H5 protein and anti-GAPDH was used as a loading control. In the lower panel, quantification of B7-H5/GAPDH is shown from three independent blots, ± SD. Statistically significant results ($p < 0.05$) are marked with an asterisk.

has been described that non-glycosylated PD-L1 undergoes faster protein degradation,[34] and the N-glycans in PD-L1 have been found to hinder recognition by PD-L1 antibodies and to reduce therapeutic efficacy, highlighting the N-glycosylation of B7 proteins as a potential therapeutic intervention mechanism in cancer.[37] The potential impact of N-glycosylation on B7-H5 in their interaction with ligands and subsequent role in immunosuppressive function, as well as in their subcellular trafficking toward the cell membrane and in their protein stability, requires further studies.

Viability analysis of renal cancer cells upon silencing B7-H5 expression resulted in a modest, but significant, decrease in their proliferation and viability in 2D and 3D growth conditions. IHC analysis revealed the significance of high B7-H5 expression on tumor cells with lower stage. This could indicate that B7-H5 plays a role in the early progression of ccRCC. In this regard, low levels of B7-H5 in ccRCC tumor cells have been

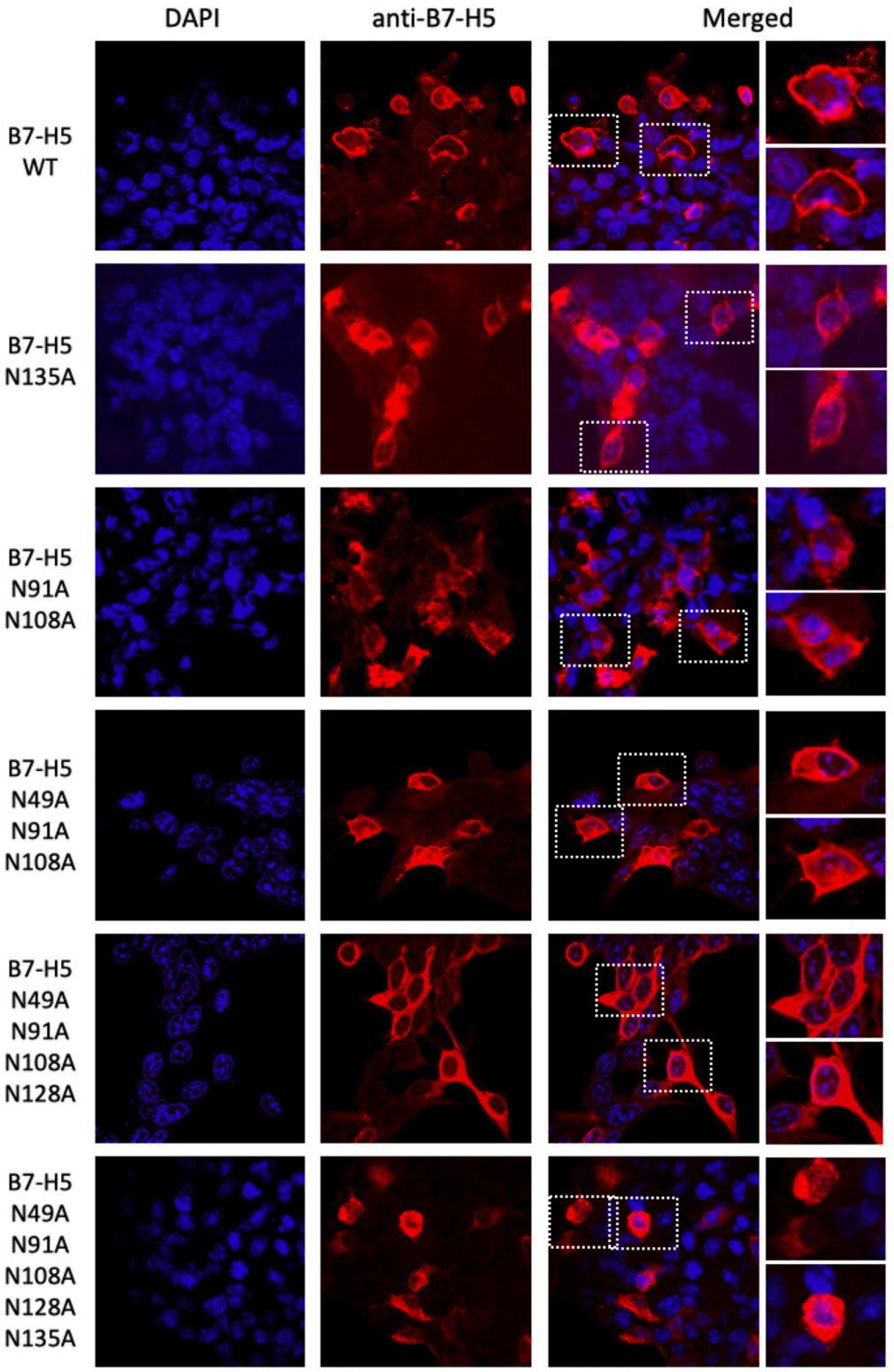

Figure 3. Protein localization of B7-H5 WT and N-glycosylation mutations

Immunofluorescence confocal microscope images at 63X showing subcellular localization of ectopically expressed B7-H5 WT and selected B7-H5 N-glycosylation mutations in HEK293 cells. Nuclei were stained with DAPI (in blue). Anti-B7-H5 primary antibody and Alexa Fluor 546 conjugated secondary antibody were used for visualization of the B7-H5 proteins (in red).

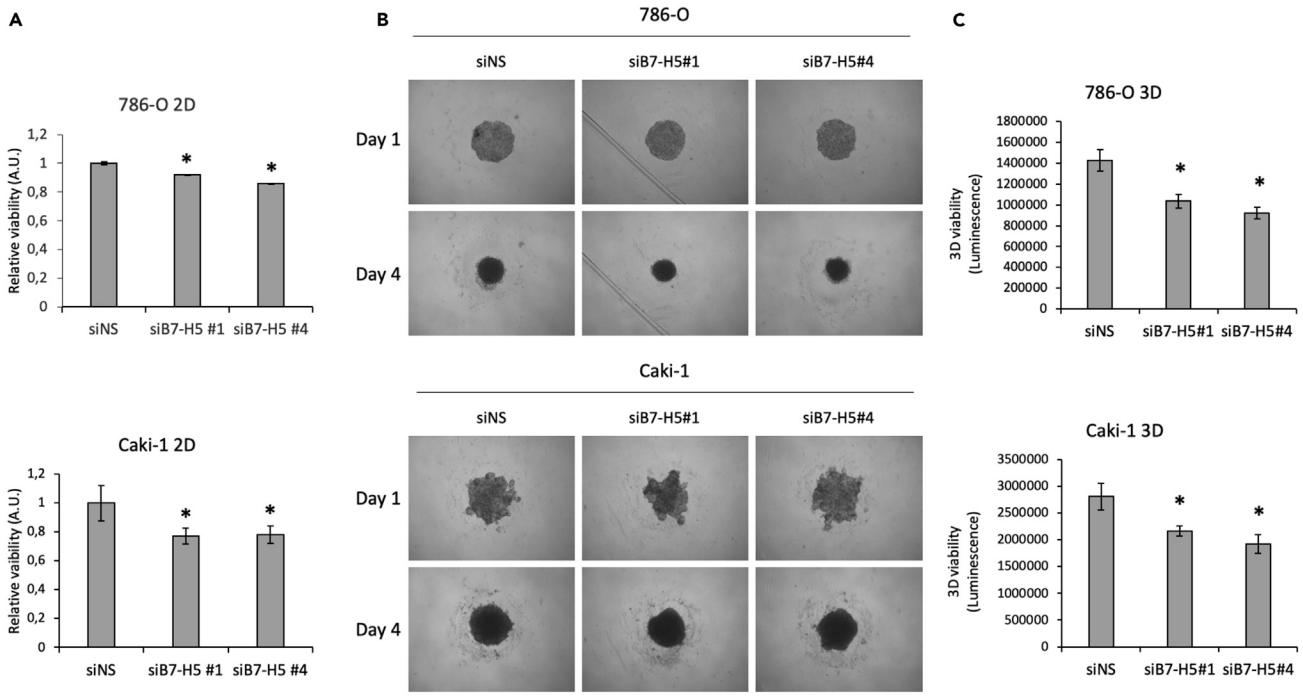

Figure 4. 2D and 3D viability of renal cancers cells upon silencing of B7-H5

(A) Relative viability of 786-O and Caki-1 cells following transfection with siNS (negative control), siB7-H5 #1 or siB7-H5 #4. Data are presented relative to the negative control.

(B) 786-O and Caki-1 cell spheroid evolution the day of transfection (Day 1) and 3 days after transfection (Day 4).

(C) 3D viability of 786-O and Caki-1 cell spheroids after transfection with siNS, siB7-H5#1 or siB7-H5#4. Data are represented from one representative experiment out of three biological replicates, with 3–6 technical replicates, ±SD. Statistically significant results ($p < 0.05$) are marked with an asterisk.

reported by others.[20] Furthermore, we observed significant correlations of B7-H5 high expression on TILs in primary tumors with several clinical parameters, including higher disease stage, lower disease-free survival, and lower overall survival. This suggests a pro-oncogenic activity for B7-H5 in ccRCC, as already described in other tumor tissues.[23] B7-H5 has previously been reported to be expressed on TILs.[38] The correlation between TILs and ccRCC clinical parameters has been studied in several investigations. High levels of TILs may not always correspond to higher antitumor activity by immune cells, as TILs may be exhausted or inactive by immune checkpoint inhibitory activity. In line with our results, B7-H5 expression in TILs in venous tumor thrombi is associated with shorter overall survival in ccRCC.[27] Immune checkpoint proteins play a critical role in tumor immune evasion, and it has been reported that tumors with T cell infiltrations have a higher success rate of immune checkpoint blockade therapy.[39] This is consistent with the results of ccRCC studies that show that lower levels of TILs were observed in metastatic tumors compared with primary tumors, which could be explained by the immunoediting and immune evasion processes these tumors undergo.[40] RCC tumors infiltrated by PD-1-expressing immune cells were reported to exhibit unfavorable pathological characteristics, such as the increased risk of cancer-specific death and overall mortality.[41] Studies of immune checkpoint inhibitors in ccRCC have mainly been focused on PD-L1 expression.

In summary, our results provide an insight into the molecular features of B7-H5 protein and suggest the potential role of B7-H5 as a new immunotherapeutic target in advanced ccRCC for patients not responding to current therapies. Recently, an *ex vivo* cultured ccRCC patient-derived tumor tissue model has been used to mimic patient responses to an anti-B7-H5 monoclonal antibody, showing promising results.[42] Furthermore, anti-B7-H5 monoclonal antibodies are under therapeutic development.[43] In this regard, clinical trials (Phase 1/2) using anti-B7-H5 monoclonal antibodies are currently ongoing for solid tumors including renal cancer (ClinicalTrials.gov Identifier: NCT04475523, NCT05864144, and NCT05708950), whose results and conclusions will be important for the future implementation of B7-H5 based therapies in ccRCC. Additional studies are required to unravel the potential oncogenicity of B7-H5 and its suitability as a therapeutic target in ccRCC.

Limitations of the study

We have identified the B7-H5 residues targeted by glycosylation using *in vitro* cultures of renal cells. It would be interesting to explore the B7-H5 glycosylation patterns in ccRCC tumors, and their association to malignancy and therapy efficacy. Our study shows a correlation between B7-H5 expression on TILs and poor outcomes in ccRCC patients. These findings require further validation with additional independent cohorts.

Table 1. Correlation between clinical and pathological variables and B7-H5 protein expression in primary tumor specimens in metastatic ccRCC

Metastatic ccRCC		PRIMARY TUMOR			
Characteristic		TUMOR		TILs	
		B7-H5 low/no	B7-H5 high	B7-H5 low/no	B7-H5 high
Patients	*N* = 54	(*N* = 41)	(*N* = 13)	(*N* = 30)	(*N* = 24)
Median follow-up time	53.5	ρ = 0.036/*p* = 0.795		ρ = −0.406/*p* = 0.002	
Months		39	61	69	22
Median age at surgery	59	ρ = −0.045/*p* = 0.749		ρ = 0.133/*p* = 0.338	
Years		59	59	59	59
Sex		ρ = 0.059/*p* = 0.671		ρ = 0.222/*p* = 0.107	
Female	15	12	3	11	4
Male	39	29	10	19	20
Age at surgery		ρ = 0.131/*p* = 0.345		ρ = 0.256/*p* = 0.061	
≤70 years	46	36	10	28	18
>70 years	8	5	3	2	6
Grade[a]		ρ = −0.326/*p* = 0.016		ρ = 0.059/*p* = 0.672	
Low	22	13	9	13	9
High	32	28	4	17	15
Stage[b]		ρ = −0.088/*p* = 0.525		ρ = 0.291/*p* = 0.033	
Low	28	20	8	19	9
High	26	21	5	11	15
Diameter[c]		ρ = 0.024/*p* = 0.863		ρ = 0.109/*p* = 0.439	
≤4 cm	9	7	2	6	3
>4 cm	44	33	11	23	24
Tumor necrosis		ρ = −0.125/*p* = 0.369		ρ = 0.382/*p* = 0.004	
No	26	18	8	18	8
Micro	8	7	1	7	1
Yes	20	16	4	5	15
Sarcomatoid transformation		ρ = 0.172/*p* = 0.215		ρ = 0.316/*p* = 0.020	
No	50	39	11	30	20
Yes	4	2	2	0	4
Disease free survival		ρ = -0.088/*p* = 0.526		ρ = 0.329/*p* = 0.015	
Yes	13	9	4	11	2
No	41	32	9	19	22
Survival		ρ = −0.106/*p* = 0.444		ρ = 0.300/*p* = 0.027	
Alive	20	14	6	15	5
Dead	34	27	7	15	19
Metastasis		ρ = 0.014/*p* = 0.920		ρ = 0.562/*p* = 0.000	
Metachronous	38	29	9	28	10
Synchronous	16	12	4	2	14

[a]Fuhrman's grade, low (G1/2) vs. high (G3/4).
[b]AJCC 2010 staging low (pT1/2) vs. high (≥pT3).
[c]Tumor diameter, small (≤4 cm) vs. large (>4 cm) Spearman correlation ρ/*p* value.

STAR★METHODS

Detailed methods are provided in the online version of this paper and include the following:

- KEY RESOURCES TABLE

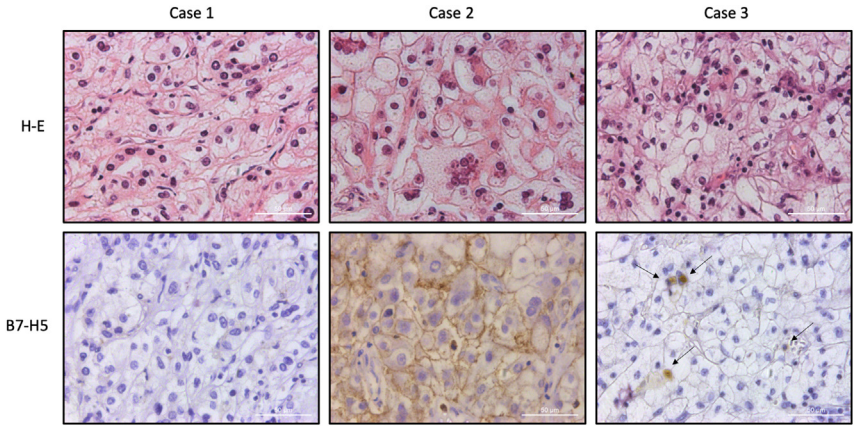

Figure 5. B7-H5 immunohistochemical expression patterns in ccRCC

Hematoxylin-eosin (H-E) staining and B7-H5 immunostaining is shown in three different ccRCC cases. Case 1 shows negative immunostaining. Case 2 shows positive immunostaining in tumor cells with a membranous pattern. Case 3 shows discrete positive immunostaining in TILs (arrows).

- RESOURCE AVAILABILITY
  - Lead contact
  - Materials availability
  - Data and code availability
- EXPERIMENTAL MODEL AND STUDY PARTICIPANT DETAILS
  - Clinical samples
- METHOD DETAILS
  - *In silico* analysis of B7 expression and potential N-glycosylation sites in renal cancer
  - Cell culture and transfections
  - Cell lysate and Western blot
  - Immunofluorescence assay
  - Silencing of B7-H5, RNA isolation, reverse transcription and RT-qPCR
  - 2D cell proliferation assay
  - Spheroid culture and 3D cell viability assay
  - Immunohistochemical staining and scoring
- QUANTIFICATION AND STATISTICAL ANALYSIS

Table 2. Correlation between clinical and pathological variables and B7-H5 protein expression in metastatic lesions in metastatic ccRCC

Metastatic ccRCC		METASTATIC SITE			
Characteristic		TUMOR		TILs	
	N=54	B7-H5 low/no	B7-H5 high	B7-H5 low/no	B7-H5 high
Patients	*N*=54	(*N*=41)	(*N*=13)	(*N*=30)	(*N*=24)
Metastatic site					
Lymph node		ρ = −0.070/*p* = 0.616		ρ = 0.195/*p* = 0.157	
No	43	32	11	26	17
Yes	11	9	2	4	7
Epithelial organs		ρ = 0.135/*p* = 0.332		ρ = −0.285/*p* = 0.037	
No	23	19	4	9	14
Yes	31	22	9	21	10
Soft tissues		ρ = −0.135/*p* = 0.329		ρ = 0.066/*p* = 0.635	
No	40	29	11	23	17
Yes	14	12	2	7	7

Spearman correlation ρ/*p* value.

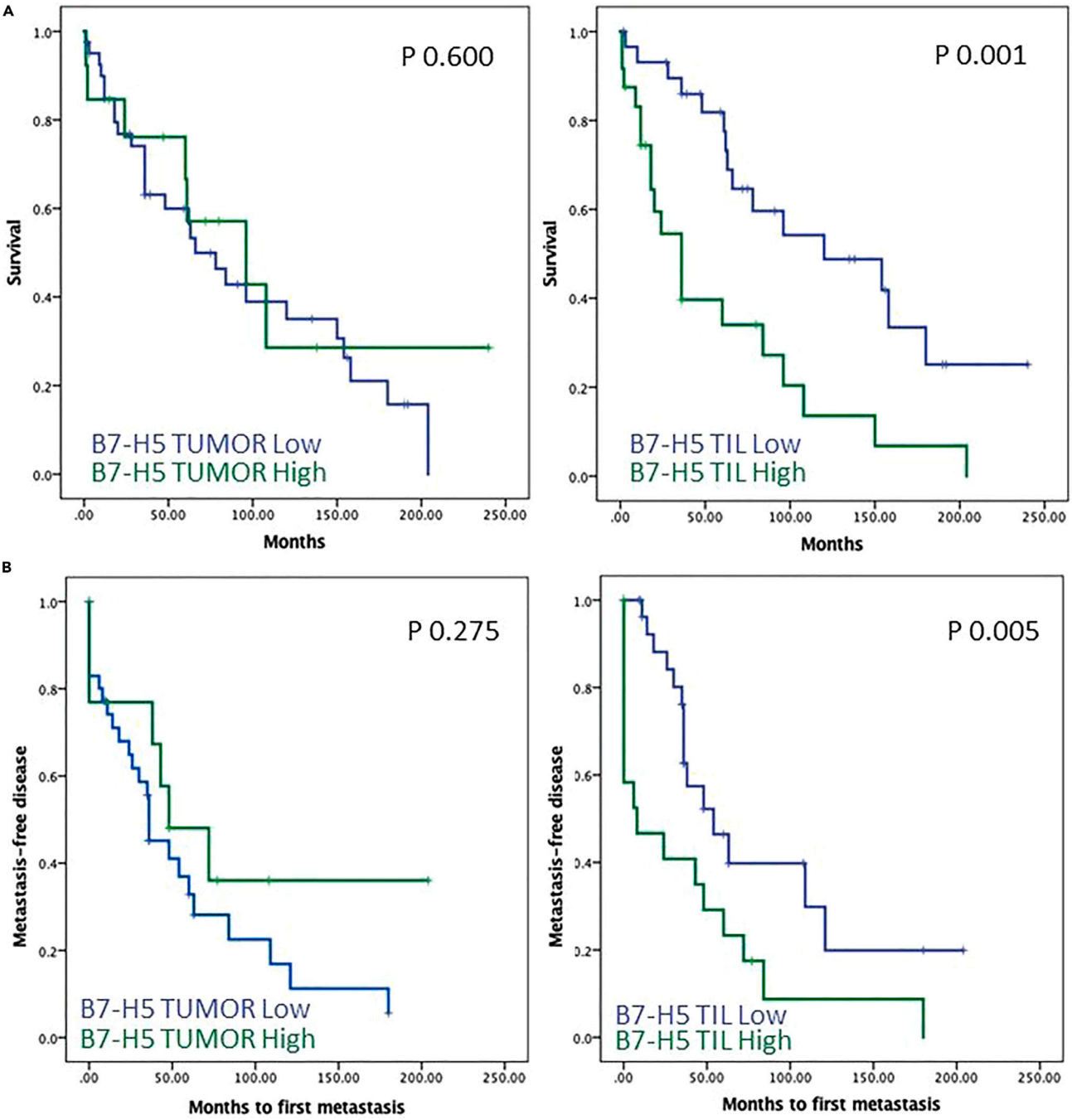

Figure 6. Kaplan-Meier survival curves of ccRCC patients according to B7-H5 expression on tumor cells and TILs

Kaplan-Meier survival curves of ccRCC patients according to overall survival (A) or metastasis-free disease (B), and B7-H5 expression on tumor cells (left panels) and TILs (right panels).

SUPPLEMENTAL INFORMATION

Supplemental information can be found online at https://doi.org/10.1016/j.isci.2024.110587.

ACKNOWLEDGMENTS

This work was funded by Instituto de Salud Carlos III grant numbers CP20/00008 and PI22/00386, (Spain and co-financed by European Union) to C.E.N-X; and Stiftelsen til fremme av forskning innen nyresykdommer/Foundation for promoting research in kidney diseases (Unifor,

Table 3. Univariate and multivariate analysis to predict overall survival of metastatic ccRCC patients

Variable	Description	Point Estimate	95% Wald Confidence Limits		p-value Log rank
Univariate analysis					
Grade	Low vs. high	1.153	0.575	2.310	0.689
Stage	Low vs. high	0.959	0.478	1.923	0.905
Diameter	<4 cm >4 cm	1.132	0.461	2.779	0.787
Tumor necrosis	No vs. yes	2.282	1.097	4.747	0.027
Sarcomatoid transformation	No vs. yes	2.828	0.635	12.595	0.173
Metastasis synchronicity	Metachronous vs. Synchronous	2.344	1.093	5.025	0.029
Metastatic site Lymph node	No vs. yes	1.826	0.730	4.569	0.198
Metastatic site Endothelial tissue	No vs. yes	0.798	0.399	1.596	0.523
Metastatic site Soft tissue, sarcoma	No vs. yes	0.883	0.408	1.907	0.751
B7-H5 tumor	No vs. yes	0.801	0.346	1.853	0.604
B7-H5 TILs	No vs. yes	2.948	1.475	5.891	0.002
Variable	**Description**	**Point Estimate**	**95% Wald Confidence Limits**		**p-value Cox**
Multivariate analysis					
Tumor necrosis	No vs. yes	2.561	1.148	5.710	0.022
Sarcomatoid transformation	No vs. yes	0.782	0.155	3.959	0.767
Metastasis synchronicity	Metachronous vs. Synchronous	1.675	0.674	4.164	0.267
B7-H5 tumor	No vs. yes	1.078	0.453	2.564	0.865
B7-H5 TILs	No vs. yes	2.780	1.294	5.973	0.009
Multivariate analysis (excluding variables with p-value > 0.2)					
Tumor necrosis	No vs. yes	2.466	1.158	5.249	0.019
B7-H5 TILs	No vs. yes	3.132	1.542	6.364	0.002

Norway) to C.E.N-X. M.E. is the recipient of a Biobizkaia Fellowship 2023/2024 (Biobizkaia Health Research Institute, Spain), and fellowships from Fundacin Jesús Gangoiti Barrera (FJGB21/006, FJGB22/006). E.R-I. is the recipient of a predoctoral fellowship from Asociación Española Contra el Cáncer (AECC, Junta Provincial de Bizkaia, Spain, PRDVZ222375REY). We would like to thank Javier Díez García (Microscope Core facility) and personnel at Genetic and Genomic Core facility for their expert assistance with microscopy and DNA sequencing, respectively, at the Biobizkaia Health Research Institute (Spain); and to Arantza Perez Dobaran (University of the Basque Country UPV/EHU, Spain) for expert technical IHC support.

AUTHOR CONTRIBUTIONS

M.E., P.A-M.: methodology, investigation, visualization, analysis, validation, and writing; E.R-I., L.M., D.L: investigation, visualization, analysis, and validation; R.P., J.I.L.: conceptualization, investigation, visualization, analysis and validation, writing - review and editing; C.E.N-X.: investigation, conceptualization, visualization, analysis, validation, supervision, funding acquisition, project administration, and writing – review, and editing.

DECLARATION OF INTERESTS

The authors declare no competing interests.

Received: March 31, 2024
Revised: June 13, 2024

Accepted: July 23, 2024
Published: July 25, 2024

REFERENCES

1. Abbott, M., and Ustoyev, Y. (2019). Cancer and the Immune System: The History and Background of Immunotherapy. Semin. Oncol. Nurs. *35*, 150923. https://doi.org/10.1016/j.soncn.2019.08.002.
2. Yang, Y. (2015). Cancer immunotherapy: harnessing the immune system to battle cancer. J. Clin. Invest. *125*, 3335–3337. https://doi.org/10.1172/JCI83871.
3. Yuan, L., Tatineni, J., Mahoney, K.M., and Freeman, G.J. (2021). VISTA: A Mediator of Quiescence and a Promising Target in Cancer Immunotherapy. Trends Immunol. *42*, 209–227. https://doi.org/10.1016/j.it.2020.12.008.
4. Huang, J.J., and Hsieh, J.J. (2020). The Therapeutic Landscape of Renal Cell Carcinoma: From the Dark Age to the Golden Age. Semin. Nephrol. *40*, 28–41. https://doi.org/10.1016/j.semnephrol.2019.12.004.
5. Xu, W., Hiếu, T., Malarkannan, S., and Wang, L. (2018). The structure, expression, and multifaceted role of immune-checkpoint protein VISTA as a critical regulator of anti-tumor immunity, autoimmunity, and inflammation. Cell. Mol. Immunol. *15*, 438–446. https://doi.org/10.1038/cmi.2017.148.
6. Johnston, R.J., Su, L.J., Pinckney, J., Critton, D., Boyer, E., Krishnakumar, A., Corbett, M., Rankin, A.L., Dibella, R., Campbell, L., et al. (2019). VISTA is an acidic pH-selective ligand for PSGL-1. Nature *574*, 565–570. https://doi.org/10.1038/s41586-019-1674-5.
7. Wang, J., Wu, G., Manick, B., Hernandez, V., Renelt, M., Erickson, C., Guan, J., Singh, R., Rollins, S., Solorz, A., et al. (2019). VSIG-3 as a ligand of VISTA inhibits human T-cell function. Immunology *156*, 74–85. https://doi.org/10.1111/imm.13001.
8. Im, E., Sim, D.Y., Lee, H.J., Park, J.E., Park, W.Y., Ko, S., Kim, B., Shim, B.S., and Kim, S.H. (2022). Immune functions as a ligand or a receptor, cancer prognosis potential, clinical implication of VISTA in cancer immunotherapy. Semin. Cancer Biol. *86*, 1066–1075. https://doi.org/10.1016/j.semcancer.2021.08.008.
9. Shekari, N., Shanehbandi, D., Kazemi, T., Zarredar, H., Baradaran, B., and Jalali, S.A. (2023). VISTA and its ligands: the next generation of promising therapeutic targets in immunotherapy. Cancer Cell Int. *23*, 265. https://doi.org/10.1186/s12935-023-03116-0.
10. Wang, L., Rubinstein, R., Lines, J.L., Wasiuk, A., Ahonen, C., Guo, Y., Lu, L.F., Gondek, D., Wang, Y., Fava, R.A., et al. (2011). VISTA, a novel mouse Ig superfamily ligand that negatively regulates T cell responses. J. Exp. Med. *208*, 577–592. https://doi.org/10.1084/jem.20100619.
11. Flies, D.B., Wang, S., Xu, H., and Chen, L. (2011). Cutting edge: A monoclonal antibody specific for the programmed death-1 homolog prevents graft-versus-host disease in mouse models. J. Immunol. *187*, 1537–1541. https://doi.org/10.4049/jimmunol.1100660.
12. Flem-Karlsen, K., Fodstad, Ø., and Nunes-Xavier, C.E. (2020). B7-H3 Immune Checkpoint Protein in Human Cancer. Curr. Med. Chem. *27*, 4062–4086. https://doi.org/10.2174/0929867326666190517115515.
13. Lines, J.L., Pantazi, E., Mak, J., Sempere, L.F., Wang, L., O'Connell, S., Ceeraz, S., Suriawinata, A.A., Yan, S., Ernstoff, M.S., and Noelle, R. (2014). VISTA is an immune checkpoint molecule for human T cells. Cancer Res. *74*, 1924–1932. https://doi.org/10.1158/0008-5472.CAN-13-1504.
14. Gao, J., Ward, J.F., Pettaway, C.A., Shi, L.Z., Subudhi, S.K., Vence, L.M., Zhao, H., Chen, J., Chen, H., Efstathiou, E., et al. (2017). VISTA is an inhibitory immune checkpoint that is increased after ipilimumab therapy in patients with prostate cancer. Nat. Med. *23*, 551–555. https://doi.org/10.1038/nm.4308.
15. Kakavand, H., Jackett, L.A., Menzies, A.M., Gide, T.N., Carlino, M.S., Saw, R.P.M., Thompson, J.F., Wilmott, J.S., Long, G.V., and Scolyer, R.A. (2017). Negative immune checkpoint regulation by VISTA: a mechanism of acquired resistance to anti-PD-1 therapy in metastatic melanoma patients. Mod. Pathol. *30*, 1666–1676. https://doi.org/10.1038/modpathol.2017.89.
16. Shi, T., Zhou, S., Zhang, T., Han, S., Zhang, L., Fu, F., Yan, R., and Zhang, X. (2022). Establishment of a Monoclonal Antibody-Based Enzyme-Linked Immunosorbent Assay to Measure Soluble B7-H5 in Patients with Cancer. J. Immunol. Res. *2022*, 3013185. https://doi.org/10.1155/2022/3013185.
17. Wu, W., Xia, X., Cheng, C., Niu, L., Wu, J., and Qian, Y. (2021). Serum Soluble PD-L1, PD-L2, and B7-H5 as Potential Diagnostic Biomarkers of Human Pancreatic Cancer. Clin. Lab. *67*, 1512. https://doi.org/10.7754/Clin.Lab.2021.210103.
18. Ghouzlani, A., Lakhdar, A., Rafii, S., Karkouri, M., and Badou, A. (2021). The immune checkpoint VISTA exhibits high expression levels in human gliomas and associates with a poor prognosis. Sci. Rep. *11*, 21504. https://doi.org/10.1038/s41598-021-00835-0.
19. Xie, X., Zhang, J., Shi, Z., Liu, W., Hu, X., Qie, C., Chen, W., Wang, Y., Wang, L., Jiang, J., and Liu, J. (2020). The Expression Pattern and Clinical Significance of the Immune Checkpoint Regulator VISTA in Human Breast Cancer. Front. Immunol. *11*, 563044. https://doi.org/10.3389/fimmu.2020.563044.
20. Hong, S., Yuan, Q., Xia, H., Zhu, G., Feng, Y., Wang, Q., Zhang, Z., He, W., Lu, J., Dong, C., and Ni, L. (2019). Analysis of VISTA expression and function in renal cell carcinoma highlights VISTA as a potential target for immunotherapy. Protein Cell *10*, 840–845. https://doi.org/10.1007/s13238-019-0642-z.
21. Zhong, C., Lang, Q., Yu, J., Wu, S., Xu, F., and Tian, Y. (2020). Phenotypical and potential functional characteristics of different immune cells expressing CD28H/B7-H5 and their relationship with cancer prognosis. Clin. Exp. Immunol. *200*, 12–21. https://doi.org/10.1111/cei.13413.
22. Deleuze, A., Saout, J., Dugay, F., Peyronnet, B., Mathieu, R., Verhoest, G., Bensalah, K., Crouzet, L., Laguerre, B., Belaud-Rotureau, M.A., et al. (2020). Immunotherapy in Renal Cell Carcinoma: The Future Is Now. Int. J. Mol. Sci. *21*, 2532. https://doi.org/10.3390/ijms21072532.
23. Noelle, R.J., Lines, J.L., Lewis, L.D., Martell, R.E., Guillaudeux, T., Lee, S.W., Mahoney, K.M., Vesely, M.D., Boyd-Kirkup, J., Nambiar, D.K., and Scott, A.M. (2023). Clinical and research updates on the VISTA immune checkpoint: immuno-oncology themes and highlights. Front. Oncol. *13*, 1225081. https://doi.org/10.3389/fonc.2023.1225081.
24. Lih, T.M., Cho, K.C., Schnaubelt, M., Hu, Y., and Zhang, H. (2023). Integrated glycoproteomic characterization of clear cell renal cell carcinoma. Cell Rep. *42*, 112409. https://doi.org/10.1016/j.celrep.2023.112409.
25. Rizzo, A., Mollica, V., Dall'Olio, F.G., Ricci, A.D., Maggio, I., Marchetti, A., Rosellini, M., Santoni, M., Ardizzoni, A., and Massari, F. (2021). Quality of life assessment in renal cell carcinoma Phase II and III clinical trials published between 2010 and 2020: a systematic review. Future Oncol. *17*, 2671–2681. https://doi.org/10.2217/fon-2021-0069.
26. Dall'Olio, F.G., Rizzo, A., Mollica, V., Massucci, M., Maggio, I., and Massari, F. (2021). Immortal time bias in the association between toxicity and response for immune checkpoint inhibitors: a meta-analysis. Immunotherapy *13*, 257–270. https://doi.org/10.2217/imt-2020-0179.
27. Zapała, Ł., Kunc, M., Sharma, S., Peksa, R., Popeda, M., Biernat, W., and Radziszewski, P. (2023). Immune checkpoint receptor VISTA on immune cells is associated with expression of T-cell exhaustion marker TOX and worse prognosis in renal cell carcinoma with venous tumor thrombus. J. Cancer Res. Clin. Oncol. *149*, 4131–4139. https://doi.org/10.1007/s00432-022-04329-y.
28. Mehta, N., Maddineni, S., Mathews, I.I., Andres Parra Sperberg, R., Huang, P.S., and Cochran, J.R. (2019). Structure and Functional Binding Epitope of V-domain Ig Suppressor of T Cell Activation. Cell Rep. *28*, 2509–2516.e5. https://doi.org/10.1016/j.celrep.2019.07.073.
29. Barata, P.C., and Rini, B.I. (2017). Treatment of renal cell carcinoma: Current status and future directions. CA. Cancer J. Clin. *67*, 507–524. https://doi.org/10.3322/caac.21411.
30. Nunes-Xavier, C.E., Angulo, J.C., Pulido, R., and López, J.I. (2019). A Critical Insight into the Clinical Translation of PD-1/PD-L1 Blockade Therapy in Clear Cell Renal Cell Carcinoma. Curr. Urol. Rep. *20*, 1. https://doi.org/10.1007/s11934-019-0866-8.
31. Baldewijns, M.M., van Vlodrop, I.J.H., Vermeulen, P.B., Soetekouw, P.M.M.B., van Engeland, M., and de Bruïne, A.P. (2010). VHL and HIF signalling in renal cell carcinogenesis. J. Pathol. *221*, 125–138. https://doi.org/10.1002/path.2689.
32. Deng, J., Li, J., Sarde, A., Lines, J.L., Lee, Y.C., Qian, D.C., Pechenick, D.A., Manivanh, R., Le Mercier, I., Lowrey, C.H., et al. (2019). Hypoxia-Induced VISTA Promotes the Suppressive Function of Myeloid-Derived Suppressor Cells in the Tumor Microenvironment. Cancer Immunol. Res. *7*, 1079–1090. https://doi.org/10.1158/2326-6066.CIR-18-0507.

33. Mulati, K., Hamanishi, J., Matsumura, N., Chamoto, K., Mise, N., Abiko, K., Baba, T., Yamaguchi, K., Horikawa, N., Murakami, R., et al. (2019). VISTA expressed in tumour cells regulates T cell function. Br. J. Cancer *120*, 115–127. https://doi.org/10.1038/s41416-018-0313-5.
34. Li, C.W., Lim, S.O., Xia, W., Lee, H.H., Chan, L.C., Kuo, C.W., Khoo, K.H., Chang, S.S., Cha, J.H., Kim, T., et al. (2016). Glycosylation and stabilization of programmed death ligand-1 suppresses T-cell activity. Nat. Commun. *7*, 12632. https://doi.org/10.1038/ncomms12632.
35. Wang, Y.N., Lee, H.H., Hsu, J.L., Yu, D., and Hung, M.C. (2020). The impact of PD-L1 N-linked glycosylation on cancer therapy and clinical diagnosis. J. Biomed. Sci. *27*, 77. https://doi.org/10.1186/s12929-020-00670-x.
36. ElTanbouly, M.A., Croteau, W., Noelle, R.J., and Lines, J.L. (2019). VISTA: a novel immunotherapy target for normalizing innate and adaptive immunity. Semin. Immunol. *42*, 101308. https://doi.org/10.1016/j.smim.2019.101308.
37. Lee, H.H., Wang, Y.N., Xia, W., Chen, C.H., Rau, K.M., Ye, L., Wei, Y., Chou, C.K., Wang, S.C., Yan, M., et al. (2019). Removal of N-Linked Glycosylation Enhances PD-L1 Detection and Predicts Anti-PD-1/PD-L1 Therapeutic Efficacy. Cancer Cell *36*, 168–178.e4. https://doi.org/10.1016/j.ccell.2019.06.008.
38. Lines, J.L., Sempere, L.F., Broughton, T., Wang, L., and Noelle, R. (2014). VISTA is a novel broad-spectrum negative checkpoint regulator for cancer immunotherapy. Cancer Immunol. Res. *2*, 510–517. https://doi.org/10.1158/2326-6066.CIR-14-0072.
39. Hendry, S., Salgado, R., Gevaert, T., Russell, P.A., John, T., Thapa, B., Christie, M., van de Vijver, K., Estrada, M.V., Gonzalez-Ericsson, P.I., et al. (2017). Assessing Tumor-infiltrating Lymphocytes in Solid Tumors: A Practical Review for Pathologists and Proposal for a Standardized Method From the International Immunooncology Biomarkers Working Group: Part 1: Assessing the Host Immune Response, TILs in Invasive Breast Carcinoma and Ductal Carcinoma In Situ, Metastatic Tumor Deposits and Areas for Further Research. Adv. Anat. Pathol. *24*, 235–251. https://doi.org/10.1097/PAP.0000000000000162.
40. Mansfield, A.S., Aubry, M.C., Moser, J.C., Harrington, S.M., Dronca, R.S., Park, S.S., and Dong, H. (2016). Temporal and spatial discordance of programmed cell death-ligand 1 expression and lymphocyte tumor infiltration between paired primary lesions and brain metastases in lung cancer. Ann. Oncol. *27*, 1953–1958. https://doi.org/10.1093/annonc/mdw289.
41. Thompson, R.H., Dong, H., Lohse, C.M., Leibovich, B.C., Blute, M.L., Cheville, J.C., and Kwon, E.D. (2007). PD-1 is expressed by tumor-infiltrating immune cells and is associated with poor outcome for patients with renal cell carcinoma. Clin. Cancer Res. *13*, 1757–1761. https://doi.org/10.1158/1078-0432.CCR-06-2599.
42. Hong, S., Yuan, Q., Xia, H., Dou, Y., Sun, T., Xie, T., Zhang, Z., He, W., Dong, C., Lu, J., et al. (2022). Establishment of an *Ex Vivo* Tissue Culture Model for Evaluation of Antitumor Efficacy in Clear Cell Renal Cell Carcinoma. Front. Oncol. *12*, 851191. https://doi.org/10.3389/fonc.2022.851191.
43. ElTanbouly, M.A., Schaafsma, E., Noelle, R.J., and Lines, J.L. (2020). VISTA: Coming of age as a multi-lineage immune checkpoint. Clin. Exp. Immunol. *200*, 120–130. https://doi.org/10.1111/cei.13415.
44. Errarte, P., Guarch, R., Pulido, R., Blanco, L., Nunes-Xavier, C.E., Beitia, M., Gil, J., Angulo, J.C., López, J.I., and Larrinaga, G. (2016). The Expression of Fibroblast Activation Protein in Clear Cell Renal Cell Carcinomas Is Associated with Synchronous Lymph Node Metastases. PLoS One *11*, e0169105. https://doi.org/10.1371/journal.pone.0169105.
45. Tang, Z., Li, C., Kang, B., Gao, G., Li, C., and Zhang, Z. (2017). GEPIA: a web server for cancer and normal gene expression profiling and interactive analyses. Nucleic Acids Res. *45*, W98–W102. https://doi.org/10.1093/nar/gkx247.
46. Mingo, J., Erramuzpe, A., Luna, S., Aurtenetxe, O., Amo, L., Diez, I., Schepens, J.T.G., Hendriks, W.J.A.J., Cortés, J.M., and Pulido, R. (2016). One-Tube-Only Standardized Site-Directed Mutagenesis: An Alternative Approach to Generate Amino Acid Substitution Collections. PLoS One *11*, e0160972. https://doi.org/10.1371/journal.pone.0160972.
47. Emaldi, M., and Nunes-Xavier, C.E. (2022). B7-H4 Immune Checkpoint Protein Affects Viability and Targeted Therapy of Renal Cancer Cells. Cells *11*, 1448. https://doi.org/10.3390/cells11091448.
48. Nunes-Xavier, C.E., Kildal, W., Kleppe, A., Danielsen, H.E., Waehre, H., Llarena, R., Maelandsmo, G.M., Fodstad, Ø., Pulido, R., and López, J.I. (2021). Immune checkpoint B7-H3 protein expression is associated with poor outcome and androgen receptor status in prostate cancer. Prostate *81*, 838–848. https://doi.org/10.1002/pros.24180.

STAR★METHODS

KEY RESOURCES TABLE

REAGENT or RESOURCE	SOURCE	IDENTIFIER
Antibodies		
Anti-FLAG	Millipore	Cat#MAB3118; RRID: AB_11213007
Anti-B7-H5/VISTA	Cell Signaling	Cat#64953; RRID: AB_2799671
Anti-GAPDH	Santa Cruz Biotechnology	Cat#sc-32233; RRID: AB_627679
Goat anti-mouse 800	Li-Cor	Cat#926-32210; RRID: AB_621842
Goat anti-rabbit 680	Li-Cor	Cat#926-68071; RRID: AB_10956166
Anti-mouse Alexa Fluor 488	Thermo Scientific	Cat#A-11001; RRID: AB_2534069
Anti-rabbit Alexa Fluor 546	Thermo Scientific	Cat#A-11060; RRID: AB_2534107
Bacterial and virus strains		
E. coli DH5alpha	Thermo Scientific	18265017
Biological samples		
Tissue microarray containing ccRCC and metastasis specimens	Cruces Hospital	NA
Critical commercial assays		
CellTiter 96® AQueous One Solution Cell Proliferation Assay (MTS)	Promega	G3581
CellTiter-Glo® 3D Cell Viability Assay	Promega	G9683
Experimental models: Cell lines		
HEK293	ATCC	CRL-1573
COS-7	ATCC	CRL-1651
786-O	ATCC	CRL-1932
Caki-1	ATCC	HTB-46
Oligonucleotides		
Primer B7-H5 N49A Forward GTCCCGAGGGGCAGGCCGTCACCCTCACCTG	Life Technologies	A1561-2
Primer B7-H5 N49A Reverse CAGGTGAGGGTGACGGCCTGCCCCTCGGGAC	Life Technologies	A1561-2
Primer B7-H5 N91A Forward CCGGCCCATCCGCGCCCTCACGTTCCAGG	Life Technologies	A1561-2
Primer B7-H5 N91A Reverse CCTGGAACGTGAGGGCGCGGATGGGCCGG	Life Technologies	A1561-2
Primer B7-H5 N108A Forward GCCACCAGGCTGCCGCCACCAGCCACGACCT	Life Technologies	A1561-2
Primer B7-H5 N108A Reverse AGGTCGTGGCTGGTGGCGGCAGCCTGGTGGC	Life Technologies	A1561-2
Primer B7-H5 N128A Forward CCGACCACCATGGCGCCTTCTCCATCACCAT	Life Technologies	A1561-2
Primer B7-H5 N128A Reverse ATGGTGATGGAGAAGGCGCCATGGTGGTCGG	Life Technologies	A1561-2
Primer B7-H5 N135A Forward CATCACCATGCGCGCCCTGACCCTGCTGG	Life Technologies	A1561-2
Primer B7-H5 N135A Reverse CCAGCAGGGTCAGGGCGCGCATGGTGATG	Life Technologies	A1561-2
Primer B7-H5 N190A Forward CCAGGATAGTGAAGCCATCACGGCTGCAG	Life Technologies	A1561-2

(*Continued on next page*)

Continued

REAGENT or RESOURCE	SOURCE	IDENTIFIER
Primer B7-H5 N190A Reverse CTGCAGCCGTGATGGCTTCACTATCCTGG	Life Technologies	A1561-2
Primer removing DYK/Flag Forward CCAAACTTTGAGGTCATCTGATAAACCCGCTGATCA	Life Technologies	A1561-2
Primer removing DYK/Flag Reverse TGATCAGCGGGTTTATCAGATGACCTCAAAGTTTGG	Life Technologies	A1561-2
Recombinant DNA		
pcDNA3.1/C-DYK/Flag B7-H5	GenScript	NM_022153.1
Software and algorithms		
GEPIA http://gepia.cancer-pku.cn	Peking University	RRID:SCR_018294
NetNGlyc http://www.cbs.dtu.dk/services/NetNGlyc/	CBS Prediction Servers	RRID:SCR_001570
Odessey Image Studio http://www.licor.com/bio/products/software/image_studio_lite/	Li-Cor	RRID:SCR_013715 v.4.0.21 software
ZEN Microscopy software https://www.zeiss.com/microscopy/en/products/software/zeiss-zen.html	ZEISS	RRID:SCR_013672
GraphPad Prism http://www.graphpad.com/	GraphPad	RRID:SCR_002798
SPSS Statistics http://www-01.ibm.com/software/uk/analytics/spss/	IBM	RRID:SCR_002865 v.29 software
Other		
DMEM	Corning	Cat#10-017-CV
RPMI 1640 medium	Corning	Cat#10-040-CV
McCoy's 5A medium	Corning	Cat#10-050-CV
FBS	Gibco	Cat#A5256701
L-Glutamine	Lonza	Cat#BE17-605E
Penicilin/Streptomycin	Lonza	Cat#DE17-602E
GenJet	SignaGen	Cat#SL100489
PBS	Corning	Cat#21-040-CV
M-PER lysis buffer	Thermo Scientific	Cat#78501
PhosStop	Roche	Cat#04 906 837 001
cOmplete protease inhibitor	Roche	Cat#04 693 132 001
PNGase F	New England Biolabs	Cat#P0704S
NuPAGE sample buffer	Thermo Scientific	Cat#NP0008
Prestained molecular marker	Sigma Aldrich	Cat#SDS7B2
Immobilon ®-FL PVDF Membrane	Merck	Cat# IPFL00010
Odyssey Blocking Buffer	Li-Cor	Cat# 927-70001
Mounting fluid with DAPI	Abcam	Cat# ab104139
PepMute	SignaGen	Cat#SL100566
siRNAs (siB7-H5#1–4)	Qiagen	Cat#1027416
dNTPs	Thermo Scientific	R0193
DpnI	Thermo Scientific	ER1701
Pwo	Roche	PWOPOL-RO
OWL HEP-1 transfer system	Thermo Scientific	Cat#HEP-1
Odyssey CLx Imager	Li-Cor	Cat#9140-09

(*Continued on next page*)

Continued

REAGENT or RESOURCE	SOURCE	IDENTIFIER
ZEISS LSM880 AIRYSCAN	Zeiss	RRID:SCR_020925
AriaMx Real-Time PCR System	Agilent Technologies	Cat#G8830A
Mark™ Microplate Absorbance Reader	Bio-Rad	Cat#168-1130
Infinite® M plex	Tecan	Cat# 30190085
PTLink	Agilent Technologies	Cat#PT100
Dako Autostainer Link 48	Agilent Technologies	Cat#AS480

RESOURCE AVAILABILITY

Lead contact

Further information and requests for resources and reagents should be directed to and will be fulfilled by the lead contact, Caroline E. Nunes-Xavier (carolinenunesxavier@gmail.com).

Materials availability

Plasmids generated in this study are available from the lead contact upon request.

Data and code availability

- This study analyzed publicly available data from the TCGA. The gene expression data are available on the GEPIA http://gepia.cancer-pku.cn.
- Uncropped original Western blot images are available as Data S1.
- This paper does not report original code.
- Any additional information required to reanalyze the data reported in this work paper is available from the lead contact upon request.

EXPERIMENTAL MODEL AND STUDY PARTICIPANT DETAILS

Clinical samples

Renal cancer cohorts with primary and metastatic ccRCC, consisted of 54 metastatic ccRCC tumors surgically removed at Cruces University Hospital in Spain between 1997 and 2001. Clinical follow-up has been recorded until October 1, 2016. FFPE blocks were preserved, and fresh tissue sections were prepared for the study. The series included primary and metastatic tissue samples from each patient. 29% of the patients had synchronous metastasis at the time of surgery, while the rest developed metachronous metastasis in a time oscillating between 6 and 204 months. The median diameter of the tumors was 8.5 cm. An experienced pathologist (JIL) selected formalin-fixed paraffin-embedded tumor areas of well-preserved tissue representative of the whole tumor from these patients, and TMA blocks were made from these areas. 4 μm sections were made from the TMA blocks, one of which was stained with hematoxylin and eosin to verify the presence and quality of tumor content. This renal cancer cohorts have been previously described in Errarte et al.[44] Ethical approval has been obtained for the clinical material (CEIm-E number PI2022085).

METHOD DETAILS

In silico analysis of B7 expression and potential N-glycosylation sites in renal cancer

The mRNA expression levels of B7-H5 in ccRCC tumor tissue was analyzed in comparison to normal tissues using samples from TCGA database via online web server GEPIA (http://gepia.cancer-pku.cn).[45] Online web server NetNGlyc (https://services.healthtech.dtu.dk/service.php?NetNGlyc-1.0) was used to identify the Asn-Xxx-Ser/Thr (N-X.S/T) motifs in B7-H5 protein sequence (NP_071436.1) which could be potential N-glycosylated sites.

Cell culture and transfections

The mammalian renal cell lines HEK293 (human embryonic kidney cell line), COS-7 (fibroblast-like cell line derived from monkey kidney tissue), and human ccRCC cell lines 786-O and Caki-1 cells were used. HEK293 and COS-7 cells were cultured in DMEM (Dulbecco's Modified Eagle's Medium, Corning), 786-O cells in RPMI 1640 medium (Corning), and Caki-1 cells in McCoy's 5A medium (Lonza). HEK293 and COS-7 cells were supplemented with 5% FBS (Fetal Bovine Serum, Gibco), and 786-O and Caki-1 cells were supplemented with 10% FBS. All medias were supplemented with 1% L-Glutamine and 1% penicillin/streptomycin (Lonza). All cells were incubated at 37°C and 5% CO_2. The vector used to ectopically express B7-H5 in mammalian cells was pcDNA3.1/C-DYK B7-H5 cDNA (NM_022153.1) (GenScript). Site-directed mutagenesis of pCDNA3.1 B7-H5 Flag was performed as described in Mingo et al.[46] and it was carried out to remove the B7-H5 C-terminal FLAG epitope

and to create B7-H5 N/A mutations. GenJet DNA *In Vitro* Transfection Reagent (SignaGen) protocol was used to transfect HEK293 and COS-7 cells with pCDNA3.1 B7-H5 Flag, or B7-H5 WT and mutations, for immunofluorescence assays and Western blot analysis.

Cell lysate and Western blot

Cells were washed twice with cold Phosphate Buffered Saline (PBS) and were lysed in lysis buffer M-PER (Mammalian Protein Extraction Reagent) (Thermo Scientific) supplemented with PhosSTOP Phosphatase Inhibitor Cocktail Tablets (Roche) and cOmplete protease inhibitor cocktail tablet (Roche). PNGase F protocol (New England Biolabs) was used to hydrolyze N-glycan chains from B7-H5 Flag, or B7-H5 WT from total cell lysates according to manufacturer's protocol. Lysates were mixed with loading buffer 4X (NuPAGE sample buffer, Life Technologies) containing 5% β-mercaptoethanol. Prestained Molecular Weight Marker (Sigma-Aldrich) was used as a molecular weight marker. Protein content in the gels was transferred to Immobilon-FL PVDF Membrane using semi-dry OWL HEP-1 transfer system (Thermo Scientific). Membranes were blocked with blocking buffer (1:1, Odyssey Blocking Buffer (OBB, Li-Cor): PBS). Primary antibodies used were mouse monoclonal anti-Flag (1:500, Flag #MAB3118, Millipore), rabbit monoclonal anti-B7-H5 (1:1000, VISTA (D1L2G) #64953, Cell Signaling), or mouse monoclonal anti-GAPDH (1:500, GAPDH (6C5) #sc-32233, SantaCruz Biotechnology). Membranes were washed with washing buffer (50 mM Tris–HCl, pH 7.5, 150 mM NaCl, 5 mM EDTA, 0.05% Triton X-100, and 0.25% gelatin) as described in Emaldi et al.[47] Secondary antibodies used were goat anti-mouse green (1:5000) or goat anti-rabbit red (1:5000). To visualize fluorescence signals on the membranes, Odyssey CLx Imager and Odyssey Image Studio v4.0.21 software (Li-Cor) were used. Data S1 contains all uncropped Western blots.

Immunofluorescence assay

HEK293 and COS-7 cells were plated in a 12-well plate and transiently transfected with plasmids to ectopically express B7-H5 Flag or B7-H5 following the GenJet^ transient transfection protocol. Cells were fixed with Metanol, and subsequently blocked in blocking solution (PBS 3% BSA). Cells were incubated with mouse anti-Flag(1:100 in blocking solution, Flag #MAB3118, Millipore), or rabbit anti-B7-H5 primary antibodies (1:100 in blocking solution, VISTA (D1L2G) #64953, Cell Signaling). Secondary antibodies used were anti-mouse Alexa Fluor 488 (1:100) or anti-rabbit Alexa Fluor 546 (1:100). Mounting fluid with DAPI (Abcam) was added for the staining of the nuclei. Visualization was seen in a confocal microscope (ZEISS LSM880 AIRYSCAN - objective 63×, 1024×1024 pixels).

Silencing of B7-H5, RNA isolation, reverse transcription and RT-qPCR

PepMute siRNA Transfection Reagent (SignaGen) protocol was used for B7-H5 silencing according to manufacturer's protocol. 786-O and Caki-1 cell lines were transfected with non-specific siRNA (siNS), glyceraldehyde-3-phosphate dehydrogenase siRNA (siGAPDH) and four different siRNAs for human B7-H5 gene (Qiagen). 786-O and Caki-1 cells were plated in 6-well plates and B7-H5 expression was silenced following PepMute silencing protocol. Total mRNA was extracted using Illustra RNAspin Mini RNA Isolation Kit following the manufacturer's protocol. Thermo Scientific RevertAid Reverse Transcriptase protocol was followed for cDNA synthesis, and Real time quantitative PCR (RT-qPCR) was performed to monitor B7-H5 mRNA expression using RealQ Plus 2× Master Mix Green with low ROX (Ampliqon), QuantiTect Primers (Qiagen) for HPRT, GAPDH and B7-H5, using Agilent AriaMx Real-Time PCR System (Agilent).

2D cell proliferation assay

3000 Caki-1 cells and 1500 786-O cells were plated per well and incubated for 24 h in 96-well plates. The next day B7-H5 expression was silenced following the Pepmute silencing protocol, and cells were incubated for 72 h. Cell proliferation was measured using CellTiter 96AQueous One Solution Cell Proliferation Assay Kit (Promega). Absorbance was measured at 490 nm using Mark Microplate Absorbance Reader (Bio-Rad). Relative proliferation was calculated by normalizing data to cells treated with siNS.

Spheroid culture and 3D cell viability assay

8000 Caki-1 and 786-O cells were plated per well in low attachment 96 well plates (Thermo Scientific) to create three-dimensional (3D) spheroids of ccRCC cells to better resemble the *in vivo* characteristics of a solid tumor. B7-H5 was silenced immediately after seeding for spheroid generation following PepMute silencing protocol. The evolution of the spheroids was photographed daily for 5 days using the ZEN Microscopy software (ZEISS). 96 h after transfection, viability of cells in 3D cell cultures was measured following the CellTiter-Glo 3D Cell Viability Assay (Promega) protocol. Luminescent signal was measured using the Infinite M plex (TECAN) plate reader.

Immunohistochemical staining and scoring

Anti-B7-H5 rabbit monoclonal antibody VISTA (D1L2G) #64953 (Cell Signaling, dilution 1:100) was used for immunohistochemistry (IHC). Immunostaining was performed in fully automated immunostainers following routine methods as explained in Nunes-Xavier et al.[48] Antigen retrieval was performed at pH 9 using PT link system (Agilent Technologies). B7-H5 immunostaining was performed with EnVision FLEX and Dako Autostainer Link 48 (Agilent). B7-H5 antibody was incubated for 30 min, followed by secondary antibody incubation for 15 min using secondary polyclonal anti-rabbit Ig/HRP (Dako), FLEX/HPR for 20 min, FLEX DAB/Sub Chromo for 10 min, and finally counterstaining with hematoxylin. Slides were dehydrated through incubations with sequentially increasing alcohol concentrations, before xylene incubated and cover-slipped. TMAs and tissue slides were evaluated manually by an experienced uropathologist (JIL). B7-H5 immunoscoring was

made following the immunoreactivity scoring system (IRS). Immunostaining for the tumor cells: low/no: <10% positive cells and 0–1 intensity; high: >10% positive cells and 2–4 intensity. Immunostaining for the TILs: low/no: <1% positive cells; high: >1% positive cells.

QUANTIFICATION AND STATISTICAL ANALYSIS

Statistical analysis of protein expression levels was performed by using a two-tailed Student's t-test and *p* values were calculated using GraphPad Prism for the differences in B7-H5/GAPDH. Standard deviation (SD) is represented in results by error bars. All experiments were performed at least twice, and results are shown from one representative experiment. *p* values smaller than 0.05 were considered significant and are indicated in results with an asterisk. The Spearman correlation was used to correlate B7-H5 expression to clinicopathologic parameters. The estimated survival curves were compared using the log rank test. Univariate and multivariate Cox correlation analysis was used to test the independent effects of variables of interest on survival. A stepwise variable selection for a Cox proportional hazards predictive model was used with an entry criterion of $p = 0.05$ and a stay value of $p = 0.2$. Correlations were calculated using SPSS Statistics V.29 (IBM). A two-sided *p* value of less than 0.05 was considered significant.